Computers & Industrial Engineering 125 (2018) 628–636

Contents lists available at ScienceDirect

Computers & Industrial Engineering

journal homepage: www.elsevier.com/locate/caie

A passive RFID tag-based locating and navigating approach for automated guided vehicle

Shaoping Lu[a], Chen Xu[b,*], Ray Y. Zhong[c], Lihui Wang[d]

[a] Department of Transport and Logistics, Shenzhen University, Shenzhen, China
[b] Institute of Intelligent Computing Science, Shenzhen University, Shenzhen, China
[c] Department of Mechanical Engineering, The University of Auckland, Auckland, New Zealand
[d] Department of Production Engineering, KTH Royal Institute of Technology, Stockholm, Sweden

ARTICLE INFO

Keywords:
RFID
AGV
Locating
Navigating
Cyber-physical systems

ABSTRACT

This research is motivated by the industrial applications of Cyber-physical System (CPS) such as smart warehouse and intelligent manufacturing which require the support of AGV (Automated Guided Vehicle). One of the key research is locating and navigating approach that should be with much flexibility for dealing with complex industrial applications. This paper takes a passive radio frequency identification (RFID) tag-based locating and navigating approach for AGV to examine the influences of tags, antennas, and environmental aspects. The approach was validated and a prototype system was built up. Several key observations are significant from the implementation and simulation study. Firstly, it is observed that adding angle reflector could eliminate the back lobe and restrain backward reflection. Secondly, RFID antenna center and the tag center should be designed at the same height could reduce the impact area of reflection. Lessons and insights from this study will be significant for industrial practitioners to implement AGVs in smart warehouse and manufacturing management.

1. Introduction

This paper is motivated by an industrial automation case that uses automated guided vehicles (AGVs) in a smart manufacturing shop floor. With the wide awareness of Industry 4.0, AGV plays an important role in facilitating material delivery so as to achieve no-human intervention automation (Herrero-Perez & Martinez-Barbera, 2010). In an AGV system, locating and navigating services are important since they greatly influence the efficiency and effectiveness of automation (Park & Lee, 2011). For example, under the Industry 4.0 smart manufacturing systems, large number of AGVs have to work seamlessly in different complex scenarios (Dessouky, 1996; Upasani, Bakshi, Pandhare, & Lad, 2017). The AGV routing based on a suitable navigation approach for avoiding congestion in the dynamic environment is becoming more and more significant (Bartlett et al., 2014).

Fixed guide paths are widely used for navigating and locating in an AGV system (Lu, Xu, & Zhong, 2016). Thus, to accommodate the AGV's paths in the workplaces, wired or wireless based systems have been employed (Luo, Ni, & Zhou, 2015). However, the workplaces may be changed frequently due to the shift of manufacturing modes and upgrading of manufacturing facilities like buffers and shelves (Zhong, Dai, Qu, Hu, & Huang, 2013). Therefore, it is necessary to make the system to be reconfigurable, flexible, and compatible (Mirbozorgi, Bahrami, Sawan, & Gosselin, 2014). To this end, Lee and DiCesare (1994) introduced an integrated a scheduling approach by using AGVs for a flexible manufacturing system (Lee & DiCesare, 1994). In this approach, centralized and distributed AGVs are modelled for materials handling and part processing.

With the development of Cyber-physical System (CPS) technologies, AGVs twining with CPS for improving the precision and efficiency are widely investigated (Bueno-Delgado, Ferrero, Gandino, Pavon-Marino, & Rebaudengo, 2013; Chen, 2009; Kehoe, Patil, Abbeel, & Goldberg, 2015; Lee, Lee, Lee, & Harashima, 2002; Sato & Sano, 2014; Wu & Zhou, 2004). CPS refers to a smart control principle of physical objects and virtual services so that an integrated system could be realized (Lee, 2008). Unlike traditional systems, a CPS-based solution has significant computational resources and advanced decision-making mechanisms so that each component is a smart object which is able to sense, interact, and react in the working space (Xu et al., 2014; Zhong et al., 2015). CPS-enabled applications have been widely reported in the areas of aerospace, automotive industry, transportation, and environmental science using different smart sensors for various purposes such as automatic pilot avionics, distributed robotics, and intelligent monitoring (Barnaghi, Sheth, Singh, & Hauswirth, 2015; Jia, Lu, Wang, Zhang, &

* Corresponding author.
E-mail addresses: szlusp@163.com (S. Lu), xuchen@szu.edu.cn (C. Xu), r.zhong@auckland.ac.nz (R.Y. Zhong), lihuiw@kth.se (L. Wang).

https://doi.org/10.1016/j.cie.2017.12.026

Available online 02 January 2018

Shen, 2015; Vellaithurai, Srivastava, Zonouz, & Berthier, 2015).

In an AGV system, locating and navigating capability for dealing with complex industrial issues with its flexibility and accurateness is significant. Radio frequency identification (RFID) might be considered due to its proofed advantages like non-contact sensing ability, high efficiency, low cost, high flexibility and configurability (Tao, Zuo, Xu, Lv, & Zhang, 2014; Tao, Zuo, Xu, & Zhang, 2014; Xu et al., 2014). RFID has been used for indoor positioning system based on a Kalman filter approach (Saab & Nakad, 2011). This system estimates neglects tag-reader angle-path loss to estimate the location and then an iterative procedure is adopted to accomplish the estimation. A mobile robot navigation method using passive RFID was introduced to locate the AGVs (Park & Hashimoto, 2009). This method is based on trigonometric functions and the IC tag's Cartesian coordinates in a regular grid-like pattern.

Several research questions still need to be investigated though many studies have been carried out to examine the locating and navigating system using RFID technology (Pasku et al., 2016; Saab & Msheik, 2016). For example, what are the impacts of RFID tags on an AGV system in terms of efficiency and precision? How to deploy the RFID tags and design the RFID antennas so as to improve the locating and navigating precision? How the working environment influences on the AGV in a real-life implementation?

In order to answer these questions, this paper takes a passive RFID tag-based locating and navigating approach for example to examine the influences of tags, antennas, and environmental aspects on an AGV system. Simulation studies are firstly carried out to examine the feasibility and practicality of the proposed approach. Based on the simulation results, a laboratory testbed is established for evaluating the system.

Several innovations are presented in this paper. First of all, Dolph-Chebyshev antenna array is used to effectively eliminate the reflection errors in the vertical direction. It is observed that adding angle reflector could eliminate the back lobe and restrain backward reflection. Secondly, it is found that the center for RFID antenna and the tag should be designed at the same height so that the reflection area will be decreased. The reflection could be controlled by adjusting the antenna radiation range. Thirdly, from the testing results in this paper, passive RFID tags should be deployed with equal space in the working environment to facilitate the AGVs' locating.

The rest of this paper is constructed as follows. Section 2 analyzes the impact factors such as tags, antenna, and environmental perspectives on far-field passive RFID system. Section 3 reports on the system design and validation of the proposed approach in theoretical perspectives. Section 4 presents the system implementation and discussions. Simulation experiment and testbed implementation are illustrated. Section 5 concludes this paper by giving our findings and future work.

2. Analysis of impact factors on far-field passive RFID system

2.1. Far-field passive RFID system

A far-field passive RFID system usually uses Ultra High Frequency (UHF) which is widely used due to its suitable cost and advantages (Bekkali, Zou, Kadri, Crisp, & Penty, 2015). Such system is capable of identifying objects with long distance and multiple items at one time (Wang, Xu, Bi, & Xu, 2014). With the identification capability, it has been widely used for supporting manufacturing operations like item-level tracking and tracing (Tao, Zuo, Xu, Lv, & Zhang, 2014; Tao, Zuo, Xu, & Zhang, 2014; Zhong, Lan, Xu, Dai, & Huang, 2016). When it works, tags are placed within the reader antenna's radiation field.

In practical application for activating the tags, circular polarization fashion is usually adopted (Zhu, Cao, Xu, Yang, & Kong, 2014). The backscatter energy transmission of passive RFID system could be demonstrated as:

$$P_r = P_t \frac{\lambda^2 G_t G_r \sigma}{(4\pi)^3 r_1^2 r_2^2} \tag{1}$$

where G_t is the gain of transmitting antenna. G_r is the gain of receiving antenna. P_r is the power of receiving antenna. P_t is the power of transmitting antenna. r_1 and r_2 are the distances between the tag and both antennas respectively. λ is the wavelength. σ is the scatter coefficient. If the transmitting and receiving antenna are the same $G_r = G_t$, (1) could be expressed as:

$$P_r = P_t \frac{\lambda^2 G^2 \sigma}{(4\pi)^3 r^4} \tag{2}$$

The gain of antenna is associated to (θ,φ) which is the directional angle. Thus, the factors effecting P_r include transmission power P_t, wavelength λ, gain of the antenna G, distance r, and the tag scatter coefficient σ. In the following section, impacts of tags and antennas are quantitatively examined.

2.2. Impact of tags

20 sets of tags with different antennas are selected for testing. Four points in the same direction are tested for each tag. 200 testing data from each tag are achieved. Fig. 1 presents the test results. It is observed that no matter how the combination of antennas changing, the generality of the tags is basically consistent. X-axis is the distance (Meter) and Y-axis is the Received Signal Strength Indication (RSSI dBm).

Tags with same type from a same manufacture are grouped such as No. 1–5, No. 6–10, and No. 11–15. The signal strengths of No. 16, No. 17 and No. 19 at various points are same, but far diverse from that of No. 18 and 20. From Fig. 1, it could be observed that different types of tags have remarkable differences on reading performance. Some tags have stronger strength, and some could not be read at all with the same distances.

Tag's posture is tested when it is detected by a reader, for example tags could be placed vertically or horizontally. For same types, their materials and surfaces are similar. But with different postures, the received radiation area would be different. Thus, the energy reflected to the receiving antenna would also be different. A test is carried out by setting the tag horizontally with same height of the antenna. For different distances from the antenna, the test is under a set of data with the tag rotation of 15° horizontally and vertically each time. Fig. 2 presents the signal strength trends with the angle changing at different rotations.

From Fig. 2, the experimental results showed that the measured tags have a feature of half-wave antenna. That means when the tag is horizontally rotated, its signal strength is a symmetric shape as a bow (Fig. 2(a)). When rotating vertically, the strengths are little smaller at the parallel plane of the tags (Fig. 2(b)). That is similar with half-wave antenna.

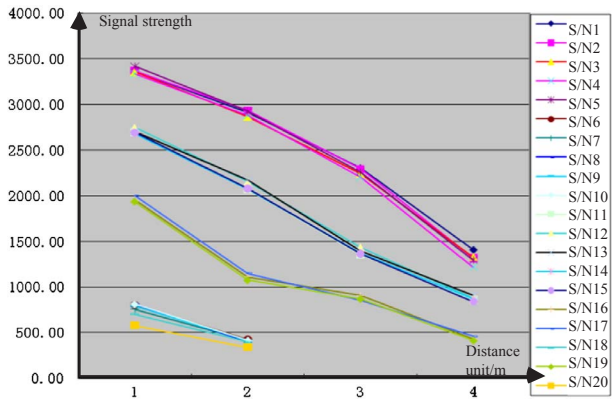

Fig. 1. Testing results of tags.

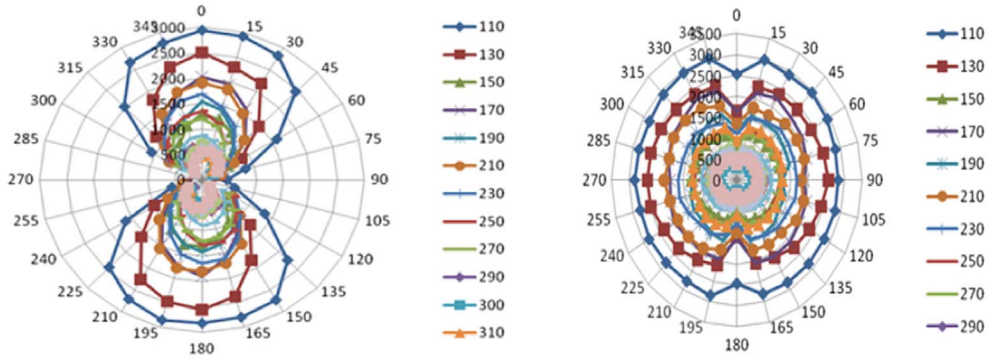

(a) Horizontal rotation (b) Vertical rotation

Fig. 2. Signal strength test results.

2.3. Impact of antenna

The analysis of antenna impact is to obtain the directional function and beam width to make the system work on a stable environment. The micro-strip patch antenna is able to produce circularly polarized wave (Qu, He, Yang, & Nie, 2014). Theoretically, when the length L and width W of a rectangle patch are content with the equation $L = W \approx 0.49\lambda$, the directional function of micro-strip patch antenna is:

$$f(\theta,\varphi) = \frac{\sin\left(\frac{\beta W}{2}\sin\theta\sin\varphi\right)}{\frac{\beta W}{2}\sin\theta\sin\varphi}\cos\left(\frac{\beta W}{2}\sin\theta\cos\varphi\right) \tag{3}$$

The directional function on surface E and surface H could be obtained using:

$$f_{\mathrm{E}}(\theta) = \cos\left(\frac{\beta W}{2}\sin\theta\right) \quad \varphi = \pi/2 \tag{4}$$

$$f_{\mathrm{H}}(\theta) = \frac{\sin\left(\frac{\beta W}{2}\sin\theta\right)}{\frac{\beta W}{2}\sin\theta}\cos\theta \quad \varphi = 0 \tag{5}$$

The first null beam width (FNBW) in the horizontal direction is close to 180°. And the FNBW in the vertical direction is close to 150°. According to the height of tags and antenna (1 m), the angle of incidence is equal to angle of reflection. Thus, $2\tan((180°-150°)/2) = 0.5359$ can be obtained. It means that the reflection will affect the signal when the distance is larger than 0.5359 m. It could be observed that the tag backscatter signals have field strength contour. The reflection will be changed along with the distances between tags and antennas. If the distance increases, the influence on the signal intensity will be increased accordingly.

Fig. 3 shows the reflected signal of a passive RFID system. When transmitted from antenna to a tag, the signal will be returned to the antenna through backscatter. During the transmission, reflections will

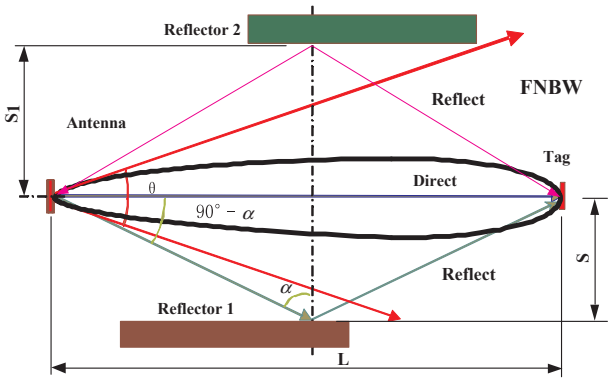

Fig. 3. The reflected signal of a passive RFID system.

be occurred. Firstly, signals could be directly transmitted from an antenna to a tag. Some background items such as equipment, floor or wall surrounding could become reflectors (reflector 1). Thus, a multi-path phenomenon will be generated. Secondly, the backscatter signals arrived at antenna include not only the direct signal, but also the reflected signals (such as the reflector 2). These reflectors may not be in the same plane, i.e. there is a main reflection signal generated by an equipment, but on the way back, the floor or ceiling will be the main reflector. According to the Snell's law, when the distance between the antenna and tags L are determined, only if the reflector is on the right midpoint, the reflected signals will not affect the signals (Nagata, Dobashi, Manabe, Usami, & Inokuchi, 1997).

Assume the distance between the tag and antenna is L, the distance between the reflector and the line of antenna and tag is S, the angle of incidence is α, there is:

$$\tan\alpha = \frac{L}{2S} \tag{6}$$

If $\frac{\theta}{2} < 90^{\circ}-\alpha$, i.e. a half of the FNBW is smaller than the complement angle of the incident angle, then:

$$\theta < 2\arctan\left(\frac{2S}{L}\right) \tag{7}$$

The reflection interruption could be omitted. Thus, we can get:

$$L < \frac{2S}{tg\left(\frac{\theta}{2}\right)} \tag{8}$$

3. System design

Based on the above analysis, this section demonstrates the system design. UHF passive tags, which have folded dipole antennas, space equally and vertically in two rows, are used to form a row of equilateral triangles tags array in the horizontal plane. Tags array is arranged along the AGV path. The distance between the tags (i.e. triangle side lengths) is determined so that the reader could cover at least three tags effectively (Lu, Xu, Zhong, & Wang, 2017). Dolph-Chebyshev antenna array and angle reflector are used to get linearly polarized signals so as to suppress the vertical reflection, horizontal reflection and environmental reflection (Zhu et al., 2014). Tags are set as the same height as the center of reader antenna. In the AGV driving process, the linear distance of the tags are relatively stable.

Tags are spaced in two rows within distance s. The distance between the two rows is $(\sqrt{3}/2) \times s$ so that they could create equilateral triangles. The vertical distance between the reader and the first tag is 1 as shown in Fig. 4. In order to ensure that at least three tags could be detected, more than one triangle should be read to cover signal intensity.

The HPBW (Half Power Beam width) angles of 60° and 90° reflector are 30° and 41° respectively. We set $l = 1 \sim 3$ m for observing the length

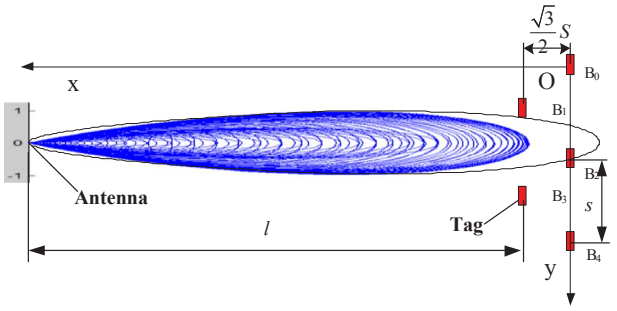

Fig. 4. Tags layout design.

Table 1
Triangle side length.

Distance	HPBW Angle	
	30°	41°
1 m	0.5359	0.7478
2 m	1.0718	1.4955
3 m	1.6077	2.2433

of triangle side. Table 1 presents the results that the triangle side length should be less than the values. According to the analysis of vertical reflection, when the distance between the antenna and the tag is 3 m, the triangle side length should be over 0.6852 m.

3.1. Antenna selection and installation design

Dolph-Chebyshev antenna array with angle planar reflector is selected because it is able to form a linear polarization. Meanwhile, it could suppress the reflections in the horizontal or vertical direction so as to cover enough number of tags (Poli, Rocca, Anselmi, & Massa, 2015). Three antenna arrays with distance $\lambda/2$ are used and planar reflector is set with 60°. The details are as follows:

Distance between the antenna array and '0' is shown in Fig. 5:
$s = 0.67 \times \lambda = 219.67$ mm
The height of antenna array: $\frac{3}{2}\lambda = \frac{3}{2} \times 327.87 = 491.8$ mm
Reflector width: $2\lambda = 2 \times 327.87 = 655.74$ mm
Height of reflector: $\frac{3}{2}\lambda + 2 \times \frac{\lambda}{2} = \frac{5}{2} \times 327.869 = 819.67$ mm

3.2. Locating solution

In Fig. 6, tags' locations (red rectangles) are set in the same height and equal spacing with the distance s. The green dot areas are the coverage of antenna. The tags' coordinates are $B_{i-1}[(\sqrt{3}s/2,0),(i-1)s/2]$,

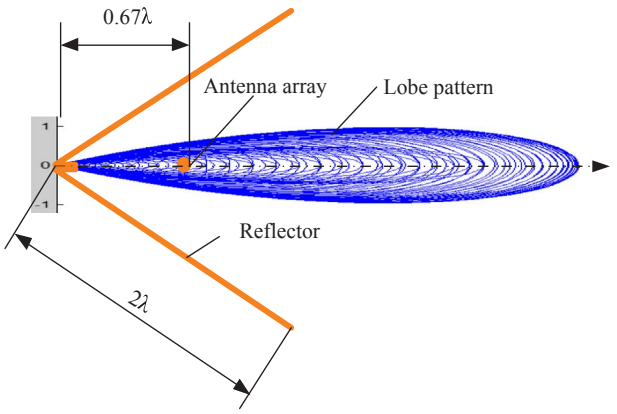

Fig. 5. Sketch of angle plate reflect.

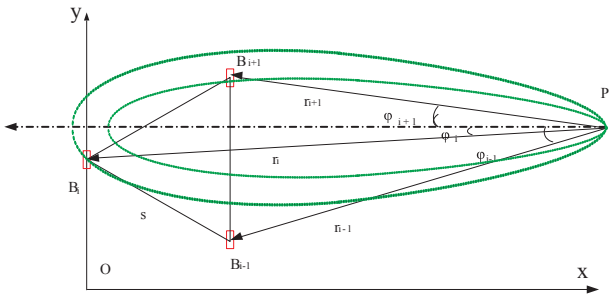

Fig. 6. Position approach of passive system.

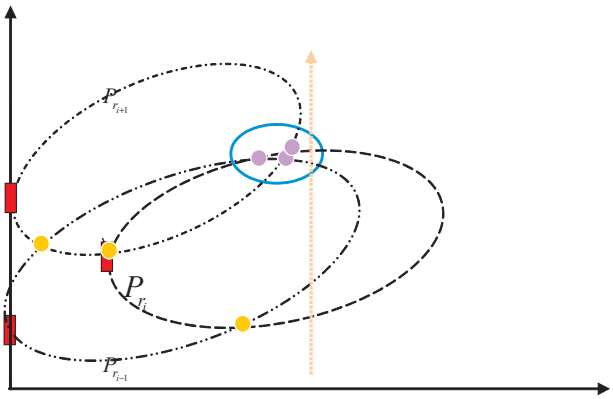

Fig. 7. Determination of an AGV location.

$B_i((0,\sqrt{3}s/2),is/2)$, and $B_{i+1}[(0,\sqrt{3}s/2),(i+1)s/2]$. $G(\varphi_i) = 2|\{\sin(S_r\cos\varphi) - \sin[S_r\cos(60^\circ - \varphi)] - \sin[S_r\cos(60^\circ + \varphi)]\}|$ is the directional function of 60° angle reflector. Details of the determination of the position could be found in Appendix. Six crossover points P_{ri} and P_{ri+1}, P_{ri} and P_{ri-1}, P_{ri+1} and P_{ri-1} could be obtained as shown in Fig. 7. The yellow points are too far beyond the range thus they are invalid. Three purple points near the AGV path are valid and their coordinates are covered by a blue circle. According to the average geometric mean method, the mean value of these three coordinates could be used to determine an AGV's location $P(X,Y)$.

After the determination, the deviation of AGV could be observed according to the predesigned driving path. In order to avoid the deviation, a threshold is set with a range of fluctuation. If the deviation is under the range, adjustment will be made by the navigation system so that AGVs are able to follow the predefined path strictly.

3.3. System verification

System verification is conducted on two aspects. First of all, theoretical analysis is focused in this section. Based on the analysis, the implementation study is conducted on next section. For the theoretical perspective, it was observed that, different antenna array have different feed and excitation methods (Maguid et al., 2016). In this paper, we take dipole direction function $F(\theta,\varphi) = \sin\theta$ for example to illustrate the validation results. θ and φ are the vertical and horizontal angle of the magnetic field. The field strength of dipole is shown in Fig. 8.

From Fig. 8, it could be observed that the space direction is an elliptical shape with a 3D dimension. The strength is stronger on the top and is becoming weaker along the vertical direction. It could be projected onto a surface so that YOZ and XOY direction graph could be obtained (as shown in Fig. 9).

From Fig. 9, it could be found that, the designed antenna array has vertical and horizontal strength since the half-power lobe width of dipole is 90° and the lobe width of first zero power is 180°. Thus, we can get the direction function of offset dipole as follows:

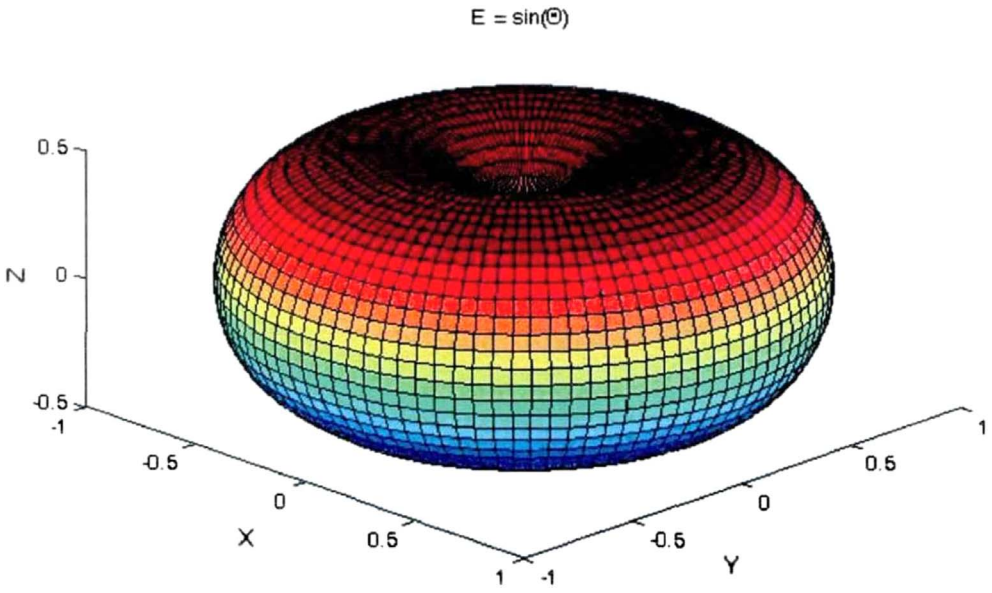

Fig. 8. Dipole Field Strength.

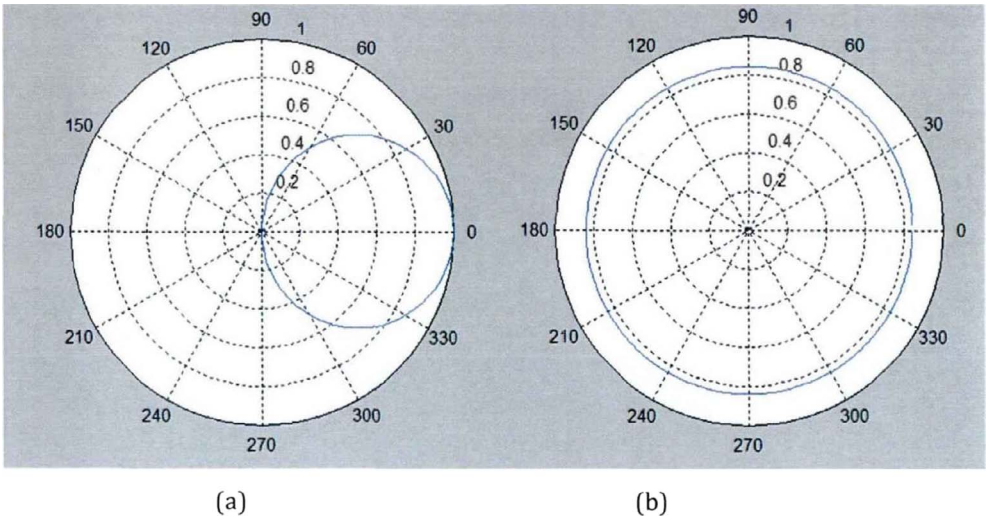

Fig. 9. Surface Direction Graph.

$$F(\theta,\varphi)=\frac{\cos\left(\frac{\beta L\cos\theta}{2}\right)-\cos\left(\frac{\beta L}{2}\right)}{\sin\theta} \tag{9}$$

When $L=\lambda/2$, we can get the half wave antenna $\beta L=\pi$ ($\beta=2\pi/\lambda$ is the phase constant). The direction function of half wave antenna is:

$$F(\theta,\varphi)=\frac{\cos(\frac{\pi\cos\theta}{2})}{\sin\theta} \tag{10}$$

Let $F(\theta,\varphi)=0.707$ which is based on the finding (>0.6852), the main lobe width is 78.12°. Let $F(\theta,\varphi)=0$, the lobe with of first zero power is 179.82°. Compared with the theoretical values of 90° and 180°, the design is feasible due to the differences of 11.88° and 0.18°.

4. System implementation and discussions

4.1. Design of experiment

The experiment design follows several steps with specific defined functions to test the feasibility and practicality of the proposed approach:

1. Initialization: (1) determine the start and end points GetPoint (); (2) initial the tags' layout and turning points SepUp (Corner, RFID);
2. Receiving signal: AGV reader is set as 500 time/s to detect tags. If more than 3 tags are detected, the tags' ID and signal density are obtained.

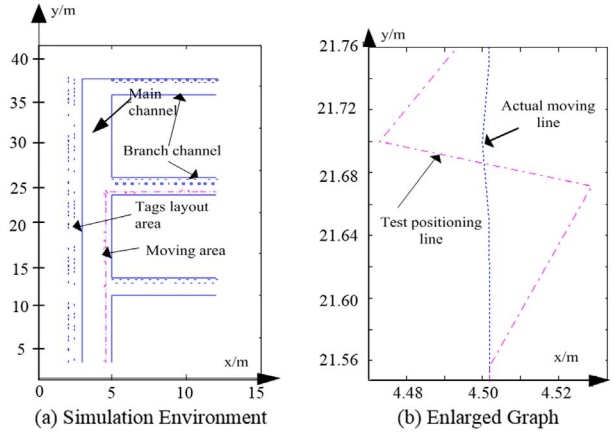

Fig. 10. Simulation results.

Table 2
Simulation testing results.

Tags	Distance (m)					
	Actual X	Actual Y	M-X	M-Y	X Error	Y Error
1	4.500	2.000	4.500	2.002	0.000	0.002
2	4.500	3.250	4.464	3.250	−0.036	0.000
3	4.500	4.500	4.505	4.482	0.005	−0.018
4	4.500	5.750	4.496	5.773	−0.005	0.023
5	4.500	7.000	4.523	6.979	0.023	−0.021
6	4.500	8.250	4.505	8.225	0.005	−0.025
7	4.500	9.500	4.500	9.510	0.000	0.009
8	4.500	10.750	4.505	10.750	0.005	0.000
9	4.500	12.000	4.500	11.988	0.000	−0.012
10	4.500	13.250	4.505	13.237	0.005	−0.013
11	4.500	14.500	4.500	14.500	0.000	0.000
12	4.500	15.750	4.505	15.750	0.005	0.000
13	4.500	17.000	4.496	17.017	−0.005	0.017
14	4.500	18.250	4.505	18.250	0.005	0.000
15	4.500	19.500	4.509	19.500	0.009	0.000
16	4.500	20.750	4.500	20.771	0.000	0.021
17	4.500	22.000	4.505	22.000	0.005	0.000
18	5.350	22.411	5.334	22.389	−0.016	−0.022
19	6.600	22.425	6.613	22.515	0.013	0.090
20	7.850	22.438	7.842	22.460	−0.008	0.022

3. Based on the tags' ID and signal density, Eqs. (A5)–(A9) are used for calculating the coordinates whose mean value is worked out for the AGV's position.

4.2. Simulation study

Simulation study with tags deployed on the wall is shown in Fig. 10, which is formed by a main corridor (main channel) and several branch corridors (branch channels). An AGV moves from the main channel into different branch channels. This simulation mainly examines the movements in main channel, detecting and steering process in the branch channels, and parking process when reached the destination. In order to prevent data accumulation, the calculating frequency (time interval) of AGV is set as 10 times/s. The speed of AGV is set as 0.5 m/s.

Fig. 10(a) shows the simulation environment with tags are deployed on the wall with the same height of antenna in the AGV. And (b) shows a zoom in view. The blue solid lines in (a) indicate the driving channel of an AGV. The blue dash line in (b) is the actual moving path. Table 2 presents a set of test results from 20 tags. The average errors of X and Y are: $\overline{|\Delta X|} = 0.016$ m and $\overline{\Delta Y} = 0.015$ m. The maximum errors are: $\Delta X_{max} = 0.023$ m and $\Delta Y_{max} = 0.090$ m.

4.3. Lab-based testbed implementation

Fig. 11 demonstrates a testbed with approximate 200 square meters in our laboratory. Three AGVs labelled as No. 1, No. 2, and No. 3 are used for testing the feasibility and practicality of the proposed locating and navigating approach. Firstly, 50 UHF passive RFID tags are placed on the ground according to the triangle distance of $(\sqrt{3}/2) \times 2.2$ m= 1.9 m. Secondly, RFID readers are deployed on each AGV with 10 cm distance to its bottom line. Thirdly, a telescopic shoring column is equipped on each AGV to move the materials from one location to another along the defined path. Finally, several AGVs are tested in the testbed to evaluate the synchronization under different scenarios: single AGV and multiple AGVs.

Fig. 12 shows testing results of a single AGV (No. 1) in the testbed with five groups of data. Each color represents a group including (x,y) and (x',y'). x,y are the predefined coordinates. x',y' are the actual position of AGV from the test. It could be observed that the differences between actual and predefined values are not significant by comparing x',x and y',y. For example, the differences from first group are $\Delta x = x' - x = 0.0845 - 0.0857 = 0.0012$. The minor differences attribute to the reading distances and straight movement. That implies the feasibility of the proposed locating and navigating approach.

Table 3 presents a test with multiple AGVs in the laboratory. Three AGVs are examined when they are working within the testing area. Pre-C is the pre-configured checking coordinates. The actual coordinates from each AGV passed are listed in Table III. The average deviations for each AGV are (0.18, 0.17), (0.12, 0.21), and (0.10, 0.22) respectively. It could be observed that the average deviations are much larger than single testing scenario. Since the limited computation resources, the coordination and synchronization of three AGVs take up more resources

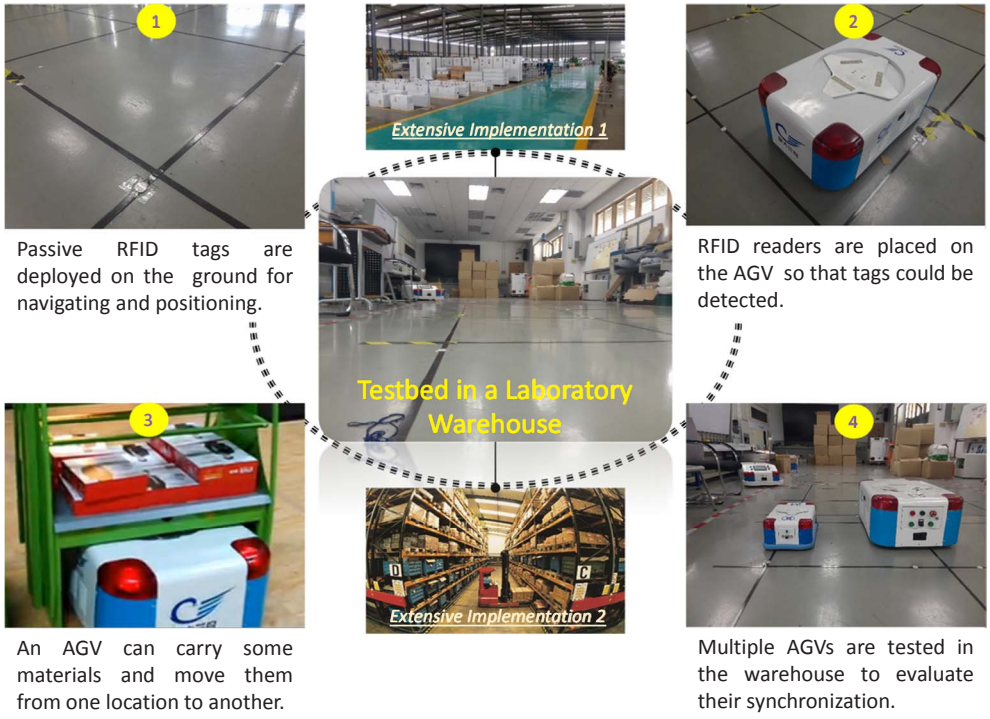

Fig. 11. A lab-based testbed implementation.

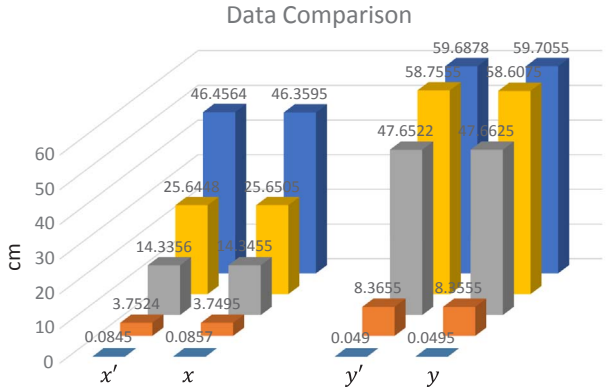

Fig. 12. Testing result of a single AGV.

Table 3
Multi-AGVs testing (Unit: m).

Pre-C	No. 1	No. 2	No. 3
(0, −0.8)	(0.05, −0.73)	(0.06, −0.82)	(0.05, −0.88)
(0, −0.2)	(0.06, −0.15)	(0.05, −0.26)	(0.06, −0.26)
(0, −0.1)	(0.02, −0.12)	(0.01, −0.14)	(0.02, −0.14)
(1.0, 0)	(1.25, 0.36)	(1.36, 0.42)	(1.35, 0.45)
(3.0, 0)	(2.88, 0.32)	(3.16, 0.35)	(3.10, 0.25)
(5.0, 0)	(5.25, 0.26)	(5.04, 0.24)	(5.10, 0.25)
(7.0, 0)	(7.36, 0.33)	(7.04, 0.40)	(7.10, 0.52)
(9.0, 0)	(9.52, 0.10)	(9.36, 0.15)	(9.10, 0.25)
(10.0, 0)	(10.0, 0.06)	(10.0, 0.24)	(10.0, 0.05)

to work out the solutions. Thus, the accuracy is decreased. Moreover, the communication using wireless standards like Bluetooth with limited network speed also attributes to the decreased accuracy in multiply testing scenario.

5. Conclusion

This paper presents a passive RFID tag-based locating and navigating approach for automated guided vehicle (AGV). The approach is based on Dolph-Chebyshev antenna array to eliminate the reflection errors efficiently. Key impact factors on far-field passive RFID system such as tags and antennas are examined in both theoretical and practical aspects. Based on the examination, this paper introduces the system design in terms of antenna selection, installation, and locating solution. The proposed approach is then evaluated by both simulation studies and a lab-based testbed where single and multiple scenarios are conducted. Several key observations or findings are significant for implementing this approach. First of all, when the distance between the antenna and the tag is 3 m, the triangle side length should be over 0.6852 m. Secondly, the reflection will affect the signal when the distance is bigger larger than 0.5359 m.

Some future research needs to be further carried out. Firstly, the tags deployment should be optimized so as to reduce the cost. Different deployment schemes like triangle, circle, and rectangle will be examined by a mathematic model. Secondly, this paper only analyzes the system in a lab-based testbed. What is the performance of this system in a real-life warehouse will be conducted. Comparisons from both lab and real-life tests will be examined to improve this approach. Finally, after implementing this system, large number of data could be collected (Zhong, Newman, Huang, & Lan, 2016). With such data, an information-driven decision support model could be established so that more precise and efficient locating and navigating could be achieved by using machine learning algorithms or models on the enormous datasets.

Acknowledgment

This work was supported by National Natural Science Foundation of China (Grant no. 61472257, 51405307, and 61401283), Guangdong Technology Plan (Grant no. 2012B010600016), Guangdong Technology Service Development Plan (Grant no. 2013B040403005), PhD Supervisor Project from Department of Education China (20134408110001), Shenzhen Governmental Project (GJHS20140418183120414) and Guangdong High Education Institution project (2013CXZDC008).

Appendix A

The determination of the position is as follows:

The coordinates of read antenna is undetermined $P(x,y)$. Then the coordinates of point P related to point B_i is:

$$\begin{cases} x = r_i\cos\varphi_i + \begin{cases} 0, & i = 0,2,4,\ldots,2n \\ \frac{\sqrt{3}}{2}s, & i = 1,3,5,\ldots,2n+1 \end{cases} \\ y = r_i\sin\varphi_i + \frac{i}{2}s \end{cases} \tag{A1}$$

According to the geometrical relationship in the graph, we can get:

$$\begin{cases} \cos(\varphi_i) = \frac{x}{r_i} \\ \cos(\varphi_{i+1}) = \frac{x - \frac{\sqrt{3}}{2}s}{r_{i+1}} \\ \sin(\varphi_{i-1}) = \frac{s}{r_i} \end{cases} \tag{A2}$$

According to Fig. 7, formula (A1) and (A2), r_i,r_{i+1},r_{i-1},φ_i,φ_{i+1},φ_{i-1} expressed by x and y could be obtained:

$$\begin{cases} r_{i+1} = \begin{cases} \sqrt{x^2 + \left[y - \frac{(i+1)s}{2}\right]^2}, i = 0,2,4,...,2n \\ \sqrt{\left(x - \frac{\sqrt{3}}{2}s\right)^2 + \left[y - \frac{(i+1)s}{2}\right]^2}, i = 1,3,5,...,2n+1 \end{cases} \\ \varphi_{i+1} = \begin{cases} \arccos \frac{x - \frac{\sqrt{3}}{2}s}{\sqrt{x^2 + \left[y - \frac{(i+1)s}{2}\right]^2}}, i = 0,2,4,...,2n \\ \arccos \frac{x - \frac{\sqrt{3}}{2}s}{\sqrt{(x - \frac{\sqrt{3}}{2}s)^2 + \left[y - \frac{(i+1)s}{2}\right]^2}}, i = 1,3,5,...,2n+1 \end{cases} \end{cases} \tag{A3}$$

$$\begin{cases} r_i = \begin{cases} \sqrt{x^2 + (y - \frac{is}{2})^2}, i = 0,2,4,...,2n \\ \sqrt{(x - \frac{\sqrt{3}}{2}s)^2 + (y - \frac{is}{2})^2}, i = 1,3,5,...,2n+1 \end{cases} \\ \varphi_i = \begin{cases} \arccos \frac{x}{\sqrt{x^2 + (y - \frac{is}{2})^2}}, i = 0,2,4,...,2n \\ \arccos \frac{x}{\sqrt{(x - \frac{\sqrt{3}}{2}s)^2 + (y - \frac{is}{2})^2}}, i = 1,3,5,...,2n+1 \end{cases} \end{cases} \tag{A4}$$

$$\begin{cases} r_{i-1} = \begin{cases} \sqrt{x^2 + \left[y - \frac{(i-1)s}{2}\right]^2}, i = 0,2,4,...,2n \\ \sqrt{\left(x - \frac{\sqrt{3}}{2}s\right)^2 + \left[y - \frac{(i-1)s}{2}\right]^2}, i = 1,3,5,...,2n+1 \end{cases} \\ \varphi_{i-1} = \begin{cases} \arcsin \frac{s}{\sqrt{x^2 + \left(y - \frac{is}{2}\right)^2}}, i = 0,2,4,...,2n \\ \arcsin \frac{s}{\sqrt{\left(x - \frac{\sqrt{3}}{2}s\right)^2 + \left(y - \frac{is}{2}\right)^2}}, i = 1,3,5,...,2n+1 \end{cases} \end{cases} \tag{A5}$$

Based on radar equation, we can get:

$$P_{r_i} = P_t \frac{\lambda^2 G^2(\varphi_i)\sigma}{(4\pi)^3 r_i^4} \tag{A6}$$

Thus, the determination of the position follows the equations:

$$\begin{cases} P_{r_i} = P_t \frac{\lambda^2 G^2(\varphi_i)\sigma}{(4\pi)^3 r_i^4} \\ P_{r_{i+1}} = P_t \frac{\lambda^2 G^2(\varphi_{i+1})\sigma}{(4\pi)^3 r_{i+1}^4} \end{cases} \tag{A7}$$

$$\begin{cases} P_{r_i} = P_t \frac{\lambda^2 G^2(\varphi_i)\sigma}{(4\pi)^3 r_i^4} \\ P_{r_{i-1}} = P_t \frac{\lambda^2 G^2(\varphi_{i-1})\sigma}{(4\pi)^3 r_{i-1}^4} \end{cases} \tag{A8}$$

$$\begin{cases} P_{r_{i-1}} = P_t \frac{\lambda^2 G^2(\varphi_{i-1})\sigma}{(4\pi)^3 r_{i-1}^4} \\ P_{r_{i+1}} = P_t \frac{\lambda^2 G^2(\varphi_{i+1})\sigma}{(4\pi)^3 r_{i+1}^4} \end{cases} \tag{A9}$$

References

Barnaghi, P., Sheth, A., Singh, V., & Hauswirth, M. (2015). Physical-cyber-social computing: looking back, looking forward. *IEEE Internet Computing, 19*(3), 7–11.

Bartlett, K., Lee, J., Ahmed, S., Nemhauser, G., Sokol, J., & Na, B. (2014). Congestion-aware dynamic routing in automated material handling systems. *Computers & Industrial Engineering, 70*, 176–182.

Bekkali, A., Zou, S., Kadri, A., Crisp, M., & Penty, R. V. (2015). Performance analysis of passive UHF RFID systems under cascaded fading channels and interference effects. *IEEE Transactions on Wireless Communications, 14*(3), 1421–1433.

Bueno-Delgado, M. V., Ferrero, R., Gandino, F., Pavon-Marino, P., & Rebaudengo, M. (2013). A geometric distribution reader anti-collision protocol for RFID dense reader environments. *IEEE Transactions on Automation Science and Engineering, 10*(2), 296–306.

Chen, W.-T. (2009). An accurate tag estimate method for improving the performance of an RFID anticollision algorithm based on dynamic frame length ALOHA. *IEEE Transactions on Automation Science and Engineering, 6*(1), 9–15.

Dessouky, I. A. (1996). Navigating the internet for engineering information. *Computers & Industrial Engineering, 31*(3–4), 889–892.

Herrero-Perez, D., & Martinez-Barbera, H. (2010). Modeling distributed transportation systems composed of flexible automated guided vehicles in flexible manufacturing systems. *IEEE Transactions on Industrial Informatics, 6*(2), 166–180.

Jia, D., Lu, K., Wang, J., Zhang, X., & Shen, X. (2015). A survey on platoon-based vehicular cyber-physical systems. *IEEE Communications Surveys & Tutorials, 18*(1), 263–284.

Kehoe, B., Patil, S., Abbeel, P., & Goldberg, K. (2015). A survey of research on cloud robotics and automation. *IEEE Transactions on Automation Science and Engineering, 12*(2), 398–409.

Lee, E. A. (2008). Cyber physical systems: Design challenges. *2008 11th IEEE international symposium on object and component-oriented real-time distributed computing (ISORC)*. IEEE.

Lee, D. Y., & DiCesare, F. (1994). Integrated scheduling of flexible manufacturing systems employing automated guided vehicles. *IEEE Transactions on Industrial Electronics,*

41(6), 602–610.
Lee, S., Lee, K. C., Lee, M. H., & Harashima, F. (2002). Integration of mobile vehicles for automated material handling using Profibus and IEEE 802.11 networks. *IEEE Transactions on Industrial Electronics, 49*(3), 693–701.
Lu, S., Xu, C., & Zhong, R. Y. (2016). An active RFID tag-enabled locating approach with multipath effect elimination in AGV. *IEEE Transactions on Automation Science and Engineering, 13*(3), 1333–1342.
Lu, S. P., Xu, C., Zhong, R. Y., & Wang, L. H. (2017). A RFID-enabled positioning system in automated guided vehicle for smart factories. *Journal of Manufacturing Systems, 44*, 179–190.
Luo, J., Ni, H., & Zhou, M. (2015). Control program design for automated guided vehicle systems via petri nets. *IEEE Transactions on Systems, Man, and Cybernetics: Systems, 45*(1), 44–55.
Maguid, E., Yulevich, I., Veksler, D., Kleiner, V., Brongersma, M. L., & Hasman, E. (2016). Photonic spin-controlled multifunctional shared-aperture antenna array. *Science,* aaf3417.
Mirbozorgi, S. A., Bahrami, H. R., Sawan, M., & Gosselin, B. (2014). A smart multicoil inductively coupled array for wireless power transmission. *IEEE Transactions on Industrial Electronics, 61*(11), 6061–6070.
Nagata, N., Dobashi, T., Manabe, Y., Usami, T., & Inokuchi, S. (1997). Modeling and visualization for a pearl-quality evaluation simulator. *IEEE Transactions on Visualization and Computer Graphics, 3*(4), 307–315.
Park, S., & Hashimoto, S. (2009). Autonomous mobile robot navigation using passive RFID in indoor environment. *IEEE Transactions on Industrial Electronics, 56*(7), 2366–2373.
Park, J., & Lee, J. (2011). A beacon color code scheduling for the localization of multiple robots. *IEEE Transactions on Industrial Informatics, 7*(3), 467–475.
Pasku, V., De Angelis, A., Dionigi, M., De Angelis, G., Moschitta, A., & Carbone, P. (2016). A Positioning system based on low-frequency magnetic fields. *IEEE Transactions on Industrial Electronics, 63*(4), 2457–2468.
Poli, L., Rocca, P., Anselmi, N., & Massa, A. (2015). Dealing with uncertainties on phase weighting of linear antenna arrays by means of interval-based tolerance analysis. *IEEE Transactions on Antennas and Propagation, 63*(7), 3229–3234.
Qu, S.-W., He, D.-J., Yang, S., & Nie, Z. (2014). Novel parasitic micro strip arrays for low-cost active phased array applications. *IEEE Transactions on Antennas and Propagation, 62*(4), 1731–1737.
Saab, S. S., & Msheik, H. (2016). Novel RFID-based pose estimation using single stationary antenna. *IEEE Transactions on Industrial Electronics, 63*(3), 1842–1852.
Saab, S. S., & Nakad, Z. S. (2011). A standalone RFID indoor positioning system using passive tags. *IEEE Transactions on Industrial Electronics, 58*(5), 1961–1970.
Sato, K., & Sano, Y. (2014). Practical and intuitive controller design method for precision positioning of a pneumatic cylinder actuator stage. *Precision Engineering, 38*(4), 703–710.
Tao, F., Zuo, Y., Xu, L. D., Lv, L., & Zhang, L. (2014). Internet of things and BOM-based life cycle assessment of energy-saving and emission-reduction of products. *IEEE Transactions on Industrial Informatics, 10*(2), 1252–1261.
Tao, F., Zuo, Y., Xu, L. D., & Zhang, L. (2014). IoT based intelligent perception and access of manufacturing resource towards cloud manufacturing. *IEEE Transactions on Industrial Informatics, 10*(2), 1547–1557.
Upasani, K., Bakshi, M., Pandhare, V., & Lad, B. K. (2017). Distributed maintenance planning in manufacturing industries. *Computers & Industrial Engineering, 108*, 1–14.
Vellaithurai, C., Srivastava, A., Zonouz, S., & Berthier, R. (2015). CPIndex: Cyber-physical vulnerability assessment for power-grid infrastructures. *IEEE Transactions on Smart Grid, 6*(2), 566–575.
Wang, L., Xu, L. D., Bi, Z., & Xu, Y. (2014). Data cleaning for RFID and WSN integration. *IEEE Transactions on Industrial Informatics, 10*(1), 408–418.
Wu, N. Q., & Zhou, M. C. (2004). Modeling and deadlock control of automated guided vehicle systems. *IEEE/ASME Transactions on Mechatronics, 9*(1), 50–57.
Xu, B. Y., Xu, L. D., Cai, H. M., Xie, C., Hu, J. Y., & Bu, F. L. (2014). Ubiquitous data accessing method in IoT-based information system for emergency medical services. *IEEE Transactions on Industrial Informatics, 10*(2), 1578–1586.
Zhong, R. Y., Dai, Q., Qu, T., Hu, G., & Huang, G. Q. (2013). RFID-enabled real-time manufacturing execution system for mass-customization production. *Robotics and Computer-Integrated Manufacturing, 29*(2), 283–292.
Zhong, R. Y., Huang, G. Q., Lan, S. L., Dai, Q. Y., Xu, C., & Zhang, T. (2015). A big data approach for logistics trajectory discovery from RFID-enabled production data. *International Journal of Production Economics, 165*, 260–272.
Zhong, R. Y., Lan, S., Xu, C., Dai, Q., & Huang, G. Q. (2016). Visualization of RFID-enabled shopfloor logistics big data in cloud manufacturing. *The International Journal of Advanced Manufacturing Technology, 84*(1), 5–16.
Zhong, R. Y., Newman, S. T., Huang, G. Q., & Lan, S. L. (2016). Big Data for supply chain management in the service and manufacturing sectors: Challenges, opportunities, and future perspectives. *Computers & Industrial Engineering, 101*, 572–591.
Zhu, W., Cao, J., Xu, Y., Yang, L., & Kong, J. (2014). Fault-tolerant RFID reader localization based on passive RFID tags. *IEEE Transactions on Parallel and Distributed Systems, 25*(8), 2065–2076.